

Focusing of Optical Vector-vortex Beams

Geo M. Philip and Nirmal K. Viswanathan*

School of Physics, University of Hyderabad, Hyderabad 500046, India

ABSTRACT

Theoretical formalism using vectorial Rayleigh diffraction integrals is developed to calculate the electric field components (E_x, E_y, E_z) of generalized vector-vortex (VV) beams of different phase and polarization characteristics as a function of propagation distance 'z' in the focal region of an axicon. This formalism is used to generate sub-wavelength spot-size (0.43λ) ultra-long length (80λ) longitudinally-polarized optical needle beam by appropriately selecting the phase and polarization characteristics of the input VV beam. The formalism is further extended to also generate purely transverse polarized beam with similar characteristics. The focusing process leads to interference between different field components of the beam resulting in the formation of C-point polarization singularities of index $l_c = \pm 1$ whose transverse characteristics evolve with propagation distance. Experimental results to support our theoretical calculations are presented along with lens focus comparison results.

Keywords: Diffraction theory, optical needle beam, axicon, spiral phase plate, polarization singularity

1. INTRODUCTION

Optical beams with spatially varying state of polarization with cylindrical symmetry are known as cylindrical vector beams [1]. As the focusing characteristics of optical beams strongly depend on the state of polarization, especially in the non-paraxial regime, the high numerical aperture (NA) focusing of vector beams results in unusual electric field distributions in the focal region [1]. For a generalized vector beam the electric field vector makes a fixed angle of δ with the radial direction [1] with $\delta=0^\circ$ for radially polarized vector beam and $\delta=90^\circ$ for azimuthally polarized vector beam. The focusing properties of radial and azimuthal polarized vector beams using high NA lenses are well studied both experimentally and theoretically [2-4]. Optical vector beam with suitably engineered polarization and phase structures can give rise to sub-wavelength spot-size non-diverging beams on high-NA focusing [5, 6]. These non-diverging vector beams are widely used in super resolution microscopy [7], laser focusing acceleration of electrons [8] and optical tweezers [9].

In addition to the spatially varying polarization the optical vector beam can also carry helical phase structure making it a vector-vortex (VV) beam. It was shown recently that focusing of annular radially polarized beam can give much smaller spot sizes [10], leading to the possibility of encoding phase structure on to vector beams to generate smaller spot sizes [6]. Focusing of VV beams can generate transversely-polarized non-diffracting beams [11]. The reduction of spot size happens at the expense of depth of focus (DOF), the sharper the focusing smaller will be the DOF. But extended DOF is needed in many applications including optical imaging. Though there are methods such as wave-front coding [12], annular illumination [13] and adaptive optics techniques [14] available to extend the focal region, the axicon lens [15] based method is one of the simple ones. Most of the studies using axicon for imaging and formation of non-diverging Bessel-Gauss beams are restricted to the scalar regime. In this work we present the axicon focusing characteristics for vector-vortex input

* Tel.: +91 40 23134337; fax: +91 40 23010227
E-mail address: nirmalsp@uohyd.ernet.in

beams, extending the usefulness of the treatment to complex phase and polarization engineered optical beam focusing. Toward this we first develop the theoretical formalism based on vectorial Rayleigh diffracting integrals to explain the focusing characteristics of generalized VV beam by an axicon.

Vector beams are also known to possess V-singularity in the beam cross section where the orientation of the linear polarization is not defined [16]. Superposition of orthogonal circularly polarized plane wave and phase dislocated beams can lead to the formation of C and L singularities where the orientation of the major axis and ellipticity of the polarization ellipse respectively are not defined [16, 17]. Though it is known that high-NA focusing of azimuthally [18] and radially [19] polarized beams lead to the generation of polarization singular (PS) beams, experimental realization of the PS patterns are difficult since the focal region in high NA focus is very small (few multiples of λ). Axicon focusing enables us to experimentally measure the PS pattern and its evolution due to the extended focal region. By solving the vectorial diffraction integrals for the focusing of generalized VV beam we explain the fine structure of field and the evolution of optical field in the focal region. The interesting aspects of axicon focusing of VV beams is to realize optical beams with purely transverse and longitudinal non-diverging beams which are explained using the developed theoretical formalism.

2. VECTOR DIFFRACTION THEORY

We use vectorial Rayleigh diffraction integrals to calculate the (x, y, z) components of the electric field vector of a vector-vortex beam focused by an axicon at any position along the axis. The schematic of the focusing system that is useful to understand the formalism is shown in Fig.1. An inhomogeneously polarized (vectorial) optical beam with a phase vortex at its center, the vector-vortex (VV) beam is focused by an axicon (A) of open angle ' α '. The input beam with such phase and polarization characteristics can be generated by passing a generalized cylindrical vector beam (CVB) through a spiral phase plate (SPP). Vectorial Rayleigh diffraction integral is used to calculate the electric field of the monochromatic electromagnetic wave at any point $E(r)$ in the beam cross section propagating in a homogeneous medium by knowing the field distribution at the input $z=0$ plane [20,21].

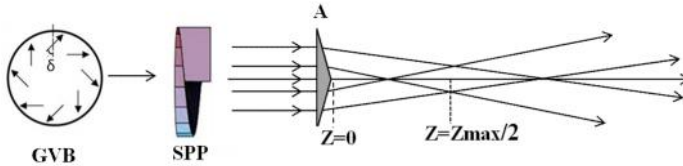


Fig. 1 Schematic of the focusing system, GVB-generalized vector beam, SPP-spiral phase plate, A-axicon, Zmax/2-centre of the non-diverging region.

The electric field components are written using the Rayleigh diffraction integral in cylindrical coordinate system as [22]

$$E_x(\rho, \beta, z) = \frac{-iz \exp(ikr)}{\lambda r^2} \int_0^\infty d\rho_0 \int_0^{2\pi} d\phi E_x(r_0) \times \exp(ik \frac{\rho_0^2}{2r}) \exp[\frac{-ik \rho \rho_0 \cos(\phi - \beta)}{r}] \rho_0 \quad (1a)$$

$$E_y(\rho, \beta, z) = \frac{-iz \exp(ikr)}{\lambda r^2} \int_0^\infty d\rho_0 \int_0^{2\pi} d\phi E_y(r_0) \times \exp(ik \frac{\rho_0^2}{2r}) \exp[\frac{-ik \rho \rho_0 \cos(\phi - \beta)}{r}] \rho_0 \quad (1b)$$

$$E_z(\rho, \beta, z) = \frac{-i \exp(ikr)}{\lambda r^2} \int_0^\infty d\rho_0 \int_0^{2\pi} d\phi [E_x(r_0)(\rho \cos \beta - \rho_0 \cos \phi) + E_y(r_0)(\rho \sin \beta - \rho_0 \sin \phi)] \times \exp(ik \frac{\rho_0^2}{2r}) \exp[\frac{-ik \rho \rho_0 \cos(\phi - \beta)}{r}] \rho_0 \quad (1c)$$

Where, (ρ, β, z) are the cylindrical coordinates at the observation point and (ρ_0, ϕ) the polar coordinates of the plane immediately after the focusing axicon. Taking into consideration the polarization aspects, the electric field of the input beam to the axicon can be written as

$$E(r_0) = \begin{pmatrix} E_x(r_0) \\ E_y(r_0) \\ E_z(r_0) \end{pmatrix} = P(\theta, \phi) A(\rho_0, \phi) \quad (2)$$

Where $P(\theta, \phi)$ is the polarization matrix and $A(\rho_0, \phi)$ is the amplitude and phase distribution of electric field after the axicon. The polarization matrix for the axicon is [23]

$$P(\theta, \phi) = \begin{pmatrix} 1 + \cos^2 \phi (\cos \theta - 1) & \sin \phi \cos \phi (\cos \theta - 1) & \cos \phi \sin \theta \\ \sin \phi \cos \phi (\cos \theta - 1) & 1 + \sin^2 \phi (\cos \theta - 1) & \sin \phi \sin \theta \\ -\sin \theta \cos \phi & -\sin \theta \sin \phi & \cos \theta \end{pmatrix} \begin{pmatrix} a(\phi, \theta) \\ b(\phi, \theta) \\ c(\phi, \theta) \end{pmatrix} \quad (3)$$

Where $a(\phi, \theta), b(\phi, \theta), c(\phi, \theta)$ are the polarization functions for x, y and z components of the incident beam. In the case of commonly used TM and TE polarized cylindrical vector beam modes these functions have a simpler form independent of θ [1]. In this work we consider paraxial input field, purely transverse in nature for which $c(\phi, \theta) = 0$. The polarization matrix (Equ. (3)) can then be rewritten as

$$P(\theta, \phi) = \begin{pmatrix} a(\theta, \phi)(\cos \theta \cos^2 \phi + \sin^2 \phi) + b(\phi, \theta)(\cos \theta - 1) \sin \phi \cos \phi \\ a(\cos \theta - 1) \sin \phi \cos \phi + b(\phi, \theta)(\cos \theta \sin^2 \phi + \cos^2 \phi) \\ -a(\theta, \phi) \sin \theta \cos \phi - \sin \theta \sin \phi \end{pmatrix} = \begin{pmatrix} P_x(\theta, \phi) \\ P_y(\theta, \phi) \\ P_z(\theta, \phi) \end{pmatrix} \quad (4)$$

Now consider the generalized VV beam with Laguerre-Gauss (LG) beam distribution incident on the axicon. The polarization state of the generalized vector beam is

$$\begin{pmatrix} a(\phi, \theta) \\ b(\phi, \theta) \\ 0 \end{pmatrix} = \begin{pmatrix} \cos(m\phi + \delta) \\ \sin(m\phi + \delta) \\ 0 \end{pmatrix} \quad (5)$$

Where 'm' denotes the order of the vector beam and ' δ ' is the phase difference between the constituent LG beams. The amplitude and phase distribution ($A(\rho_0, \phi)$) of the LG beam is [24]

$$A(\rho_0, \phi) = (\rho_0^2 / w_0^2)^{\frac{|l|}{2}} L_p^{|l|} (2 \rho_0^2 / w_0^2) \exp(\frac{\rho_0^2}{w_0^2}) \exp(il\phi) \exp(-ik\xi\rho_0) \quad (6)$$

Where $L_p^{|l|}$ is the generalized Laguerre polynomial and $\exp(-ik\xi\rho_0)$ is the axicon phase function defined as $\xi = (n-1) \tan \alpha$ (with 'n' the refractive index of the axicon material and

104 'α' the axicon open angle). Using this the electric field distribution at any point after the
 105 axicon when a generalized vector-vortex beam is focused by the axicon is written by
 106 substituting Equ.(2),(4),(5) and (6) in Equ.(1). The electric field components any point
 107 (ρ, β, z) is written as

$$108 \quad E_x(\rho, \beta, z) = \frac{-iz \exp(ikr)}{\lambda r^2} \int_0^\infty d\rho_0 \int_0^{2\pi} d\phi P_x(\phi, \theta) (\rho_0^2/w_0^2)^{\frac{|l|}{2}} L_p^{|l|}(2\rho_0^2/w_0^2) \exp(\frac{\rho_0^2}{w_0^2} + il\phi - ik\xi\rho_0 + ik\frac{\rho_0^2}{2r}) \exp[i\eta\cos(\phi - \beta)] \rho_0 \quad (7a)$$

$$109 \quad E_y(\rho, \beta, z) = \frac{-iz \exp(ikr)}{\lambda r^2} \int_0^\infty d\rho_0 \int_0^{2\pi} d\phi P_y(\phi, \theta) (\rho_0^2/w_0^2)^{\frac{|l|}{2}} L_p^{|l|}(2\rho_0^2/w_0^2) \exp(\frac{\rho_0^2}{w_0^2} + il\phi - ik\xi\rho_0 + ik\frac{\rho_0^2}{2r}) \times \exp[i\eta\cos(\phi - \beta)] \rho_0 \quad (7b)$$

$$110 \quad E_z(\rho, \beta, z) = \frac{-i \exp(ikr)}{\lambda r^2} \int_0^\infty d\rho_0 \int_0^{2\pi} d\phi [P_x(\phi, \theta)(\rho\cos\beta - \rho_0\cos\phi) + P_y(\phi, \theta)(\rho\sin\beta - \rho_0\sin\phi)] \times (\rho_0^2/w_0^2)^{\frac{|l|}{2}} L_p^{|l|}(2\rho_0^2/w_0^2) \exp(\frac{\rho_0^2}{w_0^2} + il\phi - ik\xi\rho_0 + ik\frac{\rho_0^2}{2r}) \exp[i\eta\cos(\phi - \beta)] \rho_0 \quad (7c)$$

111 Where $\eta = -k\rho\rho_0/r$.

112 The special cases for focusing of vector-vortex beams are realized by substituting the
 113 corresponding polarization matrix in the above Equ (7). The treatment presented above is
 114 valid for different types of focusing optical elements including lens and axicon and for different
 115 types of input optical beams, from plane wavefront scalar Gaussian beam to vector beam to
 116 generalized vector-vortex beam. However, as the objective of our work is to generate and
 117 understand sub-wavelength spot size focused beams with long Rayleigh range we restrict our
 118 treatment to axicon focusing of few special cases of VV beam, after verifying our results for
 119 lens focusing with already published work.

121 3.1 Lens focusing of vector-vortex beams:

122 The focusing characteristics of cylindrical vector beam by high NA lenses and the focus
 123 shaping properties are well studied using Richads-Wolf diffraction integrals [2, 3]. The
 124 mathematical formalism discussed in Section 2 is for the focusing of generalized VV beams
 125 by a conical lens, but as mentioned earlier it can be extended for lens focusing as well by
 126 incorporating the lens phase function instead of that of axicon. We used vectorial Rayleigh
 127 diffraction integral formalism to study the high NA focusing of vector-vortex beam, using the
 128 quadratic phase function for the lens: $\exp(-ik\rho^2/f)$, where 'f' is the focal length of the lens.

129 Now consider a monochromatic radially polarized beam of wavelength λ incident on the high-
 130 NA lens of focal length f. the electric field components in the focal region can be calculated by
 131 using Equ (7) after substituting $z = (z-f)$, the corresponding polarization matrix for radial
 132 polarization and the lens phase function. The simulation results obtained for focusing of
 133 radially polarized beam field using our formalism are in good agreement with the previous
 134 results[2, 3]. Fig.2 shows the normalized intensity distribution near the focal region and the
 135 contribution of different electric field components towards total intensity, when a radially
 136 polarized beam is focused by a lens of NA=0.8.

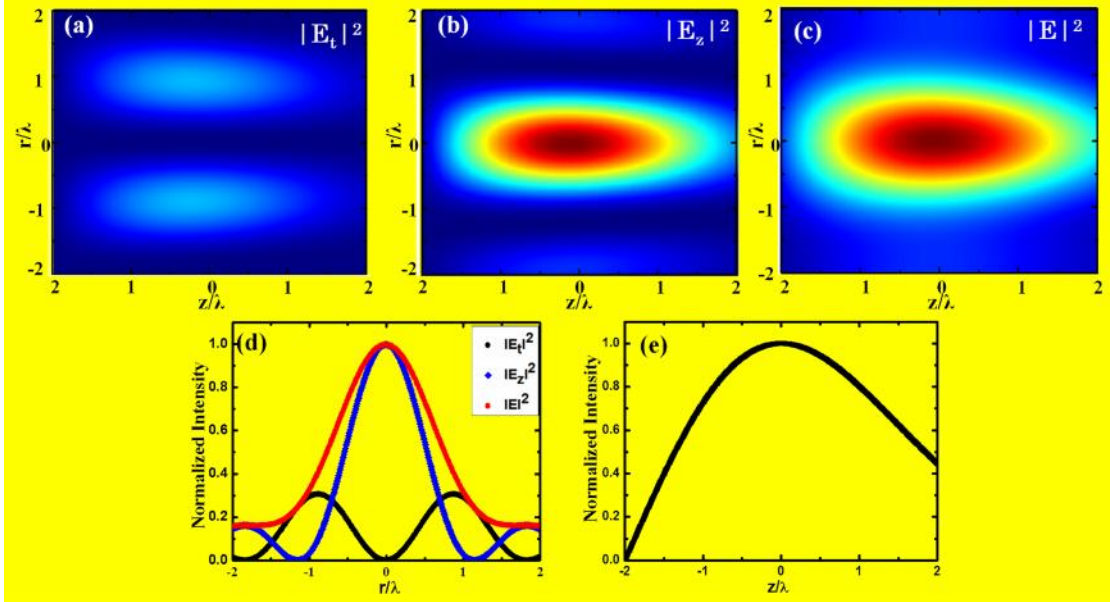


Fig. 2 (a),(b) and (c) are respectively the transverse and longitudinal field components and the total intensity with propagation; (d) shows the line profiles of the intensity distribution of (a) – (c) at the focal plane (Z=0); (e) shows the axial intensity with propagation distance.

3.2 Axicon focusing of azimuthally-polarized vortex beam:

The polarization matrix for azimuthally polarized beam is obtained by substituting $\delta = \frac{\pi}{2}$ in Equ(5), and the polarization matrix (equ (4)) then becomes

$$P(\theta, \phi) = \begin{pmatrix} \sin m\phi \\ -\cos m\phi \\ 0 \end{pmatrix} \quad (8)$$

Substituting the polarization matrix elements in Equ (7) the field components at any position after the axicon can be written as

$$E_x(\rho, \beta, z) = \frac{-iz \exp(ikr)}{\lambda r^2} \int_0^R \left(\frac{\rho_0^{l+1}}{w_0^l} \right) \exp\left(-\frac{\rho_0^2}{w_0^2}\right) L_p^{||} \left(2 \rho_0^2 / w_0^2 \right) \exp(-ik\xi\rho_0) \exp\left(ik \frac{\rho_0^2}{2r}\right) \times \quad (9a)$$

$$[\pi(-i)i^{(l+m)} J_{(l+m)}(\eta) \exp[i(l+m)\beta] + \pi i i^{(l-m)} J_{(l-m)}(\eta) \exp[i(l-m)\beta]]$$

$$E_y(\rho, \beta, z) = \frac{iz \exp(ikr)}{\lambda r^2} \int_0^R \left(\frac{\rho_0^{l+1}}{w_0^l} \right) \exp\left(-\frac{\rho_0^2}{w_0^2}\right) L_p^{||} \left(2 \rho_0^2 / w_0^2 \right) \exp(-ik\xi\rho_0) \exp\left(\frac{ik\rho_0^2}{2r}\right) \times \quad (9b)$$

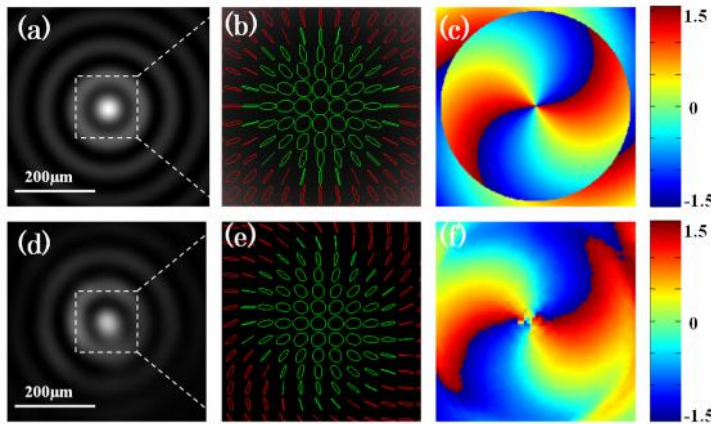
$$\{\pi i^{l+m} J_{l+m}(\eta) \exp[i(l+m)\beta] + \pi i^{l-m} J_{l-m}(\eta) \exp[i(l-m)\beta]\}$$

$$E_z(\rho, \beta, z) = \frac{i \exp(ikr)}{\lambda r^2} \int_0^R \left(\frac{\rho_0^{l+1}}{w_0^l} \right) \exp\left(-\frac{\rho_0^2}{w_0^2}\right) L_p^{||} \left(2 \rho_0^2 / w_0^2 \right) \exp(-ik\xi\rho_0) \exp\left(ik \frac{\rho_0^2}{2r}\right) \times \quad (9c)$$

$$\{\rho \pi i^{l+m} (-i) J_{l+m}(\eta) \exp[i(l+m+1)\beta] + \rho \pi i^{l-1} (i) J_{l-m}(\eta) \exp[i(l+m-1)\beta]\} d\rho_0$$

We used an azimuthally polarized beam of order $m=1$ and helical charge $l=+1$ in our experiments under low NA focusing. The vector-vortex beam generator consists of a He-Ne laser ($\lambda = 632.8$ nm) and a 27.4 cm long two-mode optical fiber. The Gaussian beam from the

156 He-Ne laser is passed through a polarizer-half wave plate combination to enable the change
 157 of the plane of polarization of the linearly polarized input beam. This linearly polarized beam is
 158 coupled skew-off axially into the circular-core step-index two-mode optical fiber ($V\# = 3.805$,
 159 length = 27.4 cm) using a 20x, 0.4 NA microscope objective lens, mounted on a 3-axis
 160 precision fiber launch system. The linear polarization of the input beam and the coupling angle
 161 are selected such that the output beam from the two-mode optical fiber is a cylindrical vector
 162 beam [25]. The output beam from the optical fiber is then collimated using 20x microscopic
 163 objective lens. Two cascaded half-wave plates are used after the collimated fiber output to
 164 rotate the spatial polarization state of the vector beam [1, 3] which in turn passes through a
 165 spiral phase plate (VPP m-633 RPC Photonics, USA) and is subsequently focused by an
 166 axicon of open angle $\alpha=0.5^\circ$. The focused beam is then imaged using a CCD along the
 167 direction of propagation 'z'. The polarization characteristics of the focused beam are
 168 measured via spatially resolved Stokes polarimetry using a quarter-wave plate and polarizer
 169 combination [26]. The generated transverse field (longitudinal field $E_z=0$) is a superposition of
 170 orthogonal circularly polarized J_0 and J_2 Bessel functions as can be seen from Eqs. (9). The
 171 beams described by the J_0 and J_2 Bessel functions have respectively a central maximum
 172 intensity and a vortex of topological charge $l = +2$ with intensity null at the centre. The on-
 173 axis superposition of the two beams with orthogonal circular polarization results in elliptically
 174 polarized field, leading to the formation of C-point and L-line in the beam cross-section [16,
 175 17]. In the present case the C-point index defined as $I_c = \frac{1}{2\pi} \oint d\psi = \pm 1$, where ψ is the
 176 polarization ellipse orientation, which rotates by 2π around the C-point. Fig.3 shows the
 177 theoretical simulations and the experimentally measured intensity distribution, polarization
 178 ellipse map and the ellipse orientation at the centre of the non-diffracting range $Z=Z_{\max}/2$,
 179 where $Z_{\max} = \omega_0 (k/k_r)$ with $k_r \approx (n-1)\alpha k$, $k=2\pi/\lambda$ is the wave vector.

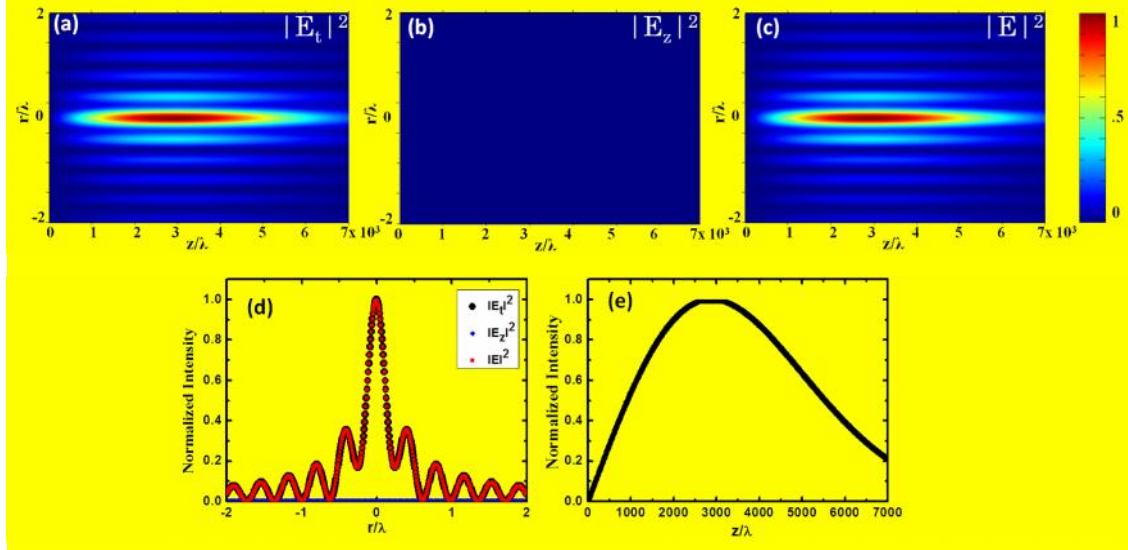


180 **Fig. 3 (a)-(c) are respectively the theoretical simulations of intensity distribution,**
 181 **polarization ellipse map and the polarization ellipse orientation. (d)-(f) are the**
 182 **corresponding experimental results, all are at $Z = Z_{\max}/2$**
 183

184 The polarization ellipse orientation around the C-point depends on the phase
 185 difference between the constituent J_0 and J_2 beams. The radial type variation in the
 186 polarization ellipse orientation around the C-point in Fig. 3 is due to the Gouy phase difference
 187 of 2π between the constituent beams with an additional Gouy phase of π added when the
 188 beams pass through the first focus [27].

189 With the simulation results (using Eqs. 9) matching the experimental results we
 190 proceed to simulate the condition when the azimuthally-polarized vector-vortex beam is
 191 focused by a high NA axicon. The focusing element is an axicon of open angle $\alpha=70^\circ$ and the
 192 input beam is an azimuthally polarized vortex beam of helical charge $l=+1$ having a waist
 193 width $\omega_0=5\text{mm}$ with $\lambda=632.8\text{nm}$. Fig.4 shows the propagation of the electric field components

194 in the focal region calculated using Equ. (9). From the figure it is seen that when an
 195 azimuthally polarized vortex beam is focused by high-NA axicon the longitudinal component of
 196 the field goes to zero resulting in a purely transverse focal field.



197 **Fig. 4 (a),(b) and (c) are respectively the transverse and longitudinal field components**
 198 **and the total intensity with propagation; (d) shows the line profiles of the intensity**
 199 **distribution of (a) – (c) at $Z=Z_{\max}/2$; (e) shows the axial intensity with propagation**
 200 **distance**
 201
 202

203 It is also important to note here that the diameter of the central spot is calculated to be
 204 0.43λ at $Z=Z_{\max}/2$ and it propagates without diverging for a long distance of (80λ) as
 205 compared to the size of the input beam and such beams are known as optical needle beam
 206 [5]. Alternate optical needle beam generation methods include focusing of phase modulated
 207 radially polarized beam by high NA lens [5], high NA lens axicon [28], focusing of radially
 208 polarized Bessel-Gauss (BG) beam [29] and reversing electric dipole array radiation [30] but
 209 all with much smaller non-diverging range than our results presented here. These long range
 210 optical needle beams find applications in polarization sensitive orientation imaging [31, 32],
 211 and light-matter interaction in the nano-scale [33]. Longitudinally polarized optical needle
 212 beams are also useful in particle manipulation and acceleration [34, 35]. It is important to note
 213 here that all these above-mentioned methods for the generation of optical needle beams [5,
 214 28-30] involve use of either complex phase modulation or amplitude modulation of the input
 215 beam. The high NA axicon based method presented here is simpler and involves direct axicon
 216 focusing of vector-vortex beam.

217 3.3 Axicon focusing of radially-polarized vortex beam:

220 Next, we extend our formalism to generate longitudinally polarized optical needle beam by
 221 focusing radially polarized vortex beam using an axicon. The polarization matrix for radial
 222 polarization is obtained by substituting $\delta = 0$ in Equ. (5) for which the polarization matrix
 223 (Equ. 4) is written as

$$P(\theta, \phi) = \begin{pmatrix} \cos \theta \cos m\phi \\ \cos \theta \sin m\phi \\ \sin \theta \end{pmatrix} \quad (10)$$

225 The electric field components after the axicon at any position along the propagation direction
 226 'Z' is obtained by substituting the polarization elements in Eqn.(7) and we get

$$227 \quad E_x(\rho, \beta, z) = \frac{-iz \exp(ikr) \cos(\theta)(\pi)}{\lambda r^2} \int_0^R \left(\frac{2\rho_0^{2|l|+1}}{w_0^{2|l|}} \right) \exp\left(-\frac{\rho_0^2}{w_0^2}\right) L_p^{|l|} \left(2\rho_0^2/w_0^2 \right) \exp(-ik\xi\rho_0) \exp\left(ik\frac{\rho_0^2}{2r}\right) \times \quad (11a)$$

$$[\pi i^{l+m} J_{l+m}(\eta) \exp(i(l+m)\beta) + \pi i^{l-m} J_{l-m}(\eta) \exp(i(l-m)\beta)] d\rho_0$$

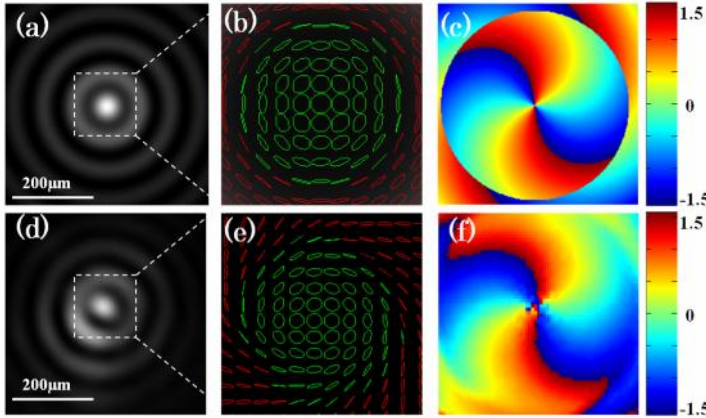
$$228 \quad E_y(\rho, \beta, z) = \frac{-iz \exp(ikr) \cos(\theta)}{\lambda r^2} \int_0^R \left(\frac{\rho_0^{l+1}}{w_0^l} \right) \exp\left(-\frac{\rho_0^2}{w_0^2}\right) L_p^{|l|} \left(2\rho_0^2/w_0^2 \right) \exp(-ik\xi\rho_0) \exp\left(ik\frac{\rho_0^2}{2r}\right) \times \quad (11b)$$

$$[\pi i^{l+m} (-i) J_{l+m}(\eta) \exp[i(l+m)\beta] + \pi i^{l-m} (i) J_{l-m}(\eta) \exp[i(l-m)\beta]] d\rho_0$$

$$229 \quad E_z(\rho, \beta, z) = \frac{i \exp(ikr) \cos \theta \exp(il\beta)}{\lambda r^2} \int_0^R \left(\frac{\rho_0^{l+1}}{w_0^l} \right) \exp\left(-\frac{\rho_0^2}{w_0^2}\right) L_p^{|l|} \left(2\rho_0^2/w_0^2 \right) \exp(-ik\xi\rho_0) \exp\left(ik\frac{\rho_0^2}{2r}\right) \times \quad (11c)$$

$$[\rho \pi i^{l+m} J_{l+m}(\eta) + \rho \pi i^{l-m} J_{l-m}(\eta) - \rho_0 2\pi i^l J_l(\eta)] d\rho_0$$

230 In our experiment the spirally polarized vector beam output from the generator is
 231 made radial by rotating the two half-wave plate orientation which is then passed through the
 232 SPP and is subsequently focused using the axicon of $\alpha=0.5^\circ$ corresponding to the case with
 233 $m=+1$, $l=+1$. Here the paraxial focus of the axicon ensures that the contribution of the
 234 longitudinal component of electric field to the total intensity is negligibly small. As before the
 235 focused beam is imaged using the CCD camera and its polarization characteristics are
 236 obtained by measuring the Stokes parameters. Fig.5 shows the theoretical simulation and
 237 experimentally measured intensity distribution, polarization ellipse map and its orientation in
 238 the middle of the non-diverging region ($Z=Z_{\max}/2$).



239

240 **Fig. 5 (a)-(c) are respectively the theoretical simulations of intensity distribution,**
 241 **polarization ellipse map and the polarization ellipse orientation. (d)-(f) are respectively**
 242 **the corresponding experimental results, all are at $Z=Z_{\max}/2$**

243 Focusing radially-polarized beam of order $m=1$ results in a central bright spot for $l=0$,
 244 1 [36], which for the $l=+1$ case is transversely polarized. To generate longitudinally polarized
 245 optical needle beam we choose radially polarized vortex beam and focus it using a high NA
 246 axicon. The electric field components can be calculated from Equ. (11). If we choose an
 247 axicon with an open angle of $\alpha=70^\circ$ the resulting longitudinally polarized central bright spot
 248 intensity is much more than the transverse component. For radially polarized vortex beam,
 249 with $l=+1$ and beam width 5mm input to the axicon Fig.6 shows the theoretically simulated

propagation characteristics. The spot size of the central bright spot is calculated to be 0.48λ and is propagating without divergence for up to a distance of 80λ .

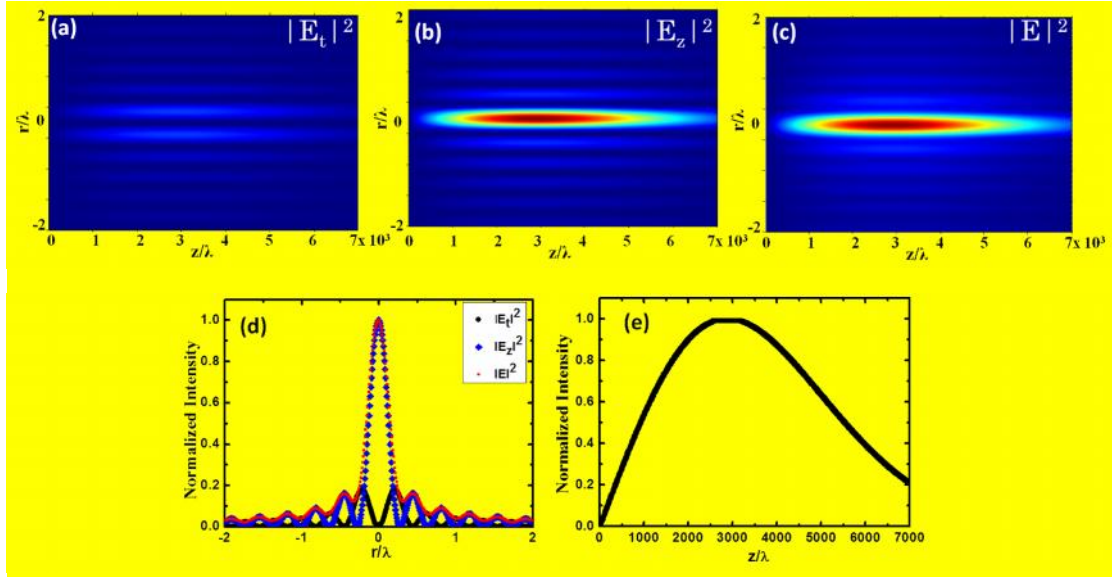


Fig. 6 (a), (b) and (c) respectively are the transverse and longitudinal components and total intensity distribution with propagation; (d) shows the line profiles of the intensity distribution of (a) – (c) at $Z=Z_{\max}/2$; (e) shows the axial intensity with propagation distance

Using the mathematical formalism developed here based on vectorial Rayleigh diffraction integrals the focusing characteristics of vector-vortex beam by an axicon is studied. The focusing of VV beam leads to the formation of polarization singularities depending on the order of the vector beam and the helical charge. It is shown that for an azimuthally polarized vortex beam the focusing leads to the formation of C-point singularity with index 1. The C-point of index 1 is formed by the superposition of J_0 and J_2 Bessel beams which are formed by adding and subtracting helical charges of the constituent beams of the cylindrical vector beam. Axicon focusing ensures longer non-diverging range where the axial phase of the beam is stationary. This ensures the polarization singular pattern free from phase distortions due to propagation. Direct generation of higher order phase vortex leads to the splitting of the helical charges but this splitting is minimum in our method. Higher-order C-points can be generated by changing the order (m) of the vector beam and by suitably adjusting the helical charge (l) of the vortex beam. For example C-point of index 2 can be generated by focusing a vector beam of order $m=2$ carrying a helical charge $l=+2$. The sign of the C-point index can also be changed by changing the handedness of the superposing Bessel beams which can be achieved by including a half wave plate after the axicon. Also, the optical needle beams generated by high NA axicon focusing of vector-vortex beams has a non-diverging range which is one order of magnitude higher than achieved by other methods.

4. CONCLUSION

A general mathematical formalism is developed for the calculation of electric field components based on vectorial Rayleigh integrals, for VV beams focused by an axicon. The formation of polarization singularities by focusing VV beam by the axicon is studied theoretically and experiments were performed to validate the theoretical predictions under low NA focus

conditions. The C-point of index 1 with different polarization ellipse structures were generated experimentally by low NA focusing of azimuthal and radial polarized VV beams. The formalism is extended to high NA axicon focusing of VV beams resulting in the generation of purely transverse or purely longitudinally polarized optical needle beams. It is shown using theoretical simulations that our method can generate optical needle beam of spot-size (0.43λ) with long non-diverging range of 80λ .

286

287 **ACKNOWLEDGEMENTS**

288 The authors acknowledge Department of Science and Technology (DST), India for financial
289 support for the project. GMP acknowledges Council of Scientific and Industrial Research
290 (CSIR), India for research fellowship.

291 **COMPETING INTERESTS**

292

293 Authors declare that no competing interests exist.

294

295 **AUTHORS' CONTRIBUTIONS**

296

297 The first author of the paper (GMP) is a research (PhD) student who carried out all the
298 calculations, simulations and experiments under the supervision of the second author (NKV).
299 The draft versions of the manuscript were written by GMP and corrected by NKV. Both
300 authors have read and approved final manuscript.

301

302 **CONSENT (WHERE EVER APPLICABLE)**

303

304 Not applicable.

305

306 **ETHICAL APPROVAL (WHERE EVER APPLICABLE)**

307

308 Not applicable.

309

310 **REFERENCES**

- 311 1. Qiwen Zhan. Cylindrical vector beams: from mathematical concepts to applications.
312 Advances in Optics and Photonics, 2009; 1: 1–57.
- 313 2. Youngworth, K. S., & Brown, T. G. Focusing of high numerical aperture cylindrical vector
314 beams. Opt. Exp 2000; 7: 77–87.
- 315 3. Qiwen Zhan and James Leger Focus shaping using cylindrical vector beams Opt. Exp
316 2002; 10: 324–331.
- 317 4. R. Dorn, S. Quabis and G. Leuchs. Sharper focus for a radially polarized light beam. Phys.
318 Rev. Lett. 2003; 91: 233901.
- 319 5. Haifeng Wang, Luping Shi, Boris Luk'yanchuk¹, Colin Sheppard and Chong Tow Chong.
320 Creation of a needle of longitudinally polarized light in vacuum using binary optics. Nature
321 Photonics 2008; 2: 501.
- 322 6. G. H. Yuan, S. B. Wei and X.-C. Yuan Nondiffracting transversally polarized beam. Opt.
323 Lett. 2011; 36: 3479–3481.

- 324 7. K. I. Willing, S. O. Rizzoli, V. Westphal, R. Jahn and S. W. Hell, STED-microscopy reveals
325 that synaptotagmin remains clustered after synaptic vesicle exocytosis. *Nature* 2006; 440:
326 935.
- 327 8. R. D. Romea and W. D. Kimura Modeling of inverse Čerenkov laser acceleration with
328 axicon laser-beam focusing. *Phys. Rev. D* 1990; 42: 1807.
- 329 9. Lu Huang, Honglian Guo, Jiafang Li, Lin Ling, Baohua Feng, and Zhi-Yuan Li. Optical
330 trapping of gold nanoparticles by cylindrical vector beam. *Opt. Lett* 2012; 37: 1694-1696.
- 331 10. Liangxin Yang, Xiangsheng Xie, Sicong Wang and Jianying Zhou. Minimized spot of
332 annular radially polarized focusing beam. *Opt. Lett* 2013; 38: 1331-1333.
- 333 11. G. H. Yuan, S. B. Wei and X.-C. Yuan. Non-diffracting transversally polarized beam. *Opt.*
334 *Lett* 2011; 36: 3479-3481.
- 335 12. E. R. Dowski, Jr. and W. T. Cathey. Extended depth of field through wave-front coding.
336 *Appl. Opt.* 1995; 34(11): 1859–1866.
- 337 13. E. J. Botcherby, R. Juškaitis, and T. Wilson. Scanning two photon fluorescence
338 microscopy with extended depth of field. *Opt. Commun.* 2006; 268(2): 253–260.
- 339 14. Kazuhiro Sasaki, Kazuhiro Kurokawa, Shuichi Makita, and Yoshiaki Yasuno. Extended
340 depth of focus adaptive optics spectral domain optical coherence tomography. *Opt. Exp* 2012;
341 3: 2353-2370.
- 342 15. P. Dufour, M. Piché, Y. De Koninck, and N. McCarthy. Two-photon excitation fluorescence
343 microscopy with a high depth of field using an axicon. *Appl. Opt.* 2006; 45(36): 9246–9252.
- 344 16. Isaac Freund. Polarization singularity indices in Gaussian laser beams. *Opt. Commun.*
345 2002; 201: 251–270.
- 346 17. Florian Flossmann, Kevin O'Holleran, Mark R. Dennis and Miles J. Padgett. Polarization
347 Singularities in 2D and 3D Speckle Fields. *Phys. Rev. Lett.* 2008; 100: 203902(1–4).
- 348 18. W. Zhang, S. Liu, P. Li, X. Jiao and J. Zhao. Controlling the polarization singularities of the
349 focused azimuthally polarized beams. *Opt. Exp.* 2013; 21: 974 – 983.
- 350 19. R. W. Schoonover and T. D. Visser. Polarization singularities of focused, radially polarized
351 fields. *Opt. Exp* 2006; 14(12): 5733–5745.
- 352 20. A. Ciattoni, B. Crosignani, and P. D. Porto. Vectorial analytical description of propagation
353 of a highly nonparaxial beam. *Opt. Commun.* 2002; 202: 17–20.
- 354 21. R. K. Luneburg, *Mathematical Theory of Optics* (University of California Press, Berkeley,
355 1966)
- 356 22. Yaoju Zhang, Ling Wang and Chongwei Zheng. Vector propagation of radially polarized
357 Gaussian beams diffracted by an axicon. *J. Opt. Soc. Am. A* 2005; 22: 2542-2546.
- 358 23. S. N. Khonina, N. L. Kazanskiy, and S. G. Volotovskiy. Influence of Vortex Transmission
359 Phase Function on Intensity Distribution in the Focal Area of High-Aperture Focusing System.
360 *Optical Memory and Neural Networks (Information Optics)* 2011 20: 23–42.
- 361 24. J. Arit and K. Dholakia. Generation of high-order Bessel beams by use of an axicon. *Opt.*
362 *Commun.* 2000; 177: 297.
- 363 25. Nirmal K. Viswanathan and V. V. G. Inavalli. Generation of optical vector beams using a
364 two-mode fiber. *Opt. Lett.* 2009; 34: 1189-1191.
- 365 26. D. H. Goldstein and E. Collett, *Polarized Light*, 2nd ed. (Marcel Dekker, 2003).
- 366 27. G.M. Philip, Vijay Kumar, Giovanni Milione, and N.K. Viswanathan. Manifestation of the
367 Gouy phase in vector-vortex beams. *Opt. Lett.* 2012; 37: 2667-2669.
- 368 28. Suresh P, Mariyal C, Rajesh KB, Pillai TV, Jaroszewicz Z. Generation of a strong uniform
369 transversely polarized nondiffracting beam using a high-numerical-aperture lens axicon with a
370 binary phase mask. *Appl Opt.* 2013; 52(4): 849-853.
- 371 29. Yikun Zha, Jingsong Wei, Haifeng Wang and Fuxi Gan. Creation of an ultra-long depth of
372 focus super-resolution longitudinally polarized beam with a ternary optical element. *J. Opt.*
373 2013; 15: 075703.
- 374 30. Jiming Wang, Weibin Chen and Qiwen Zhan. Engineering of high purity ultra-long optical
375 needle field through reversing the electric dipole array radiation. *Opt. Expr.* 2010; 18: 21965 –
376 21972.

- 377 31. A. F. Abouraddy and K. C. Toussaint, Jr. Three-dimensional polarization control in
378 microscopy. *Phys. Rev. Lett.* 2006; 96(15): 153901.
- 379 32. L. Novotny, M. R. Beversluis, K. S. Youngworth, and T. G. Brown. Longitudinal field
380 modes probed by single molecules. *Phys. Rev. Lett.* 2001; 86(23): 5251–5254.
- 381 33. P. Banzer, U. Peschel, S. Quabis, and G. Leuchs. On the experimental investigation of the
382 electric and magnetic response of a single nano-structure. *Opt. Exp* 2010; 18(10): 10905–
383 10923.
- 384 34. S. Takeuchi, R. Sugihara, and K. Shimoda. Electron acceleration by longitudinal electric
385 field of a Gaussian laser beam. *J. Phys. Soc. Jpn.* 1994; 63(3): 1186–1193.
- 386 35. M. E. J. Friese, T. A. Nieminen, N. R. Heckenberg, and H. Rubinsztein-Dunlop. Optical
387 alignment and spinning of laser-trapped microscopic particles. *Nature* 1998; 394(6691): 348–
388 350.
- 389 36. L.E. Helseth. Optical vortices in focal regions. *Opt. Commun.* 2004; 229:85-91.